Fish-like three-dimensional swimming with an autonomous, multi-fin, and biomimetic robot

F. Berlinger[1*], M. Saadat[2], H. Haj-Hariri[3], G. V. Lauder[2], R. Nagpal[1]

Supplementary Material

Finbot is the first autonomous and biomimetic multi-fin platform with closed-loop sensing and control that is small enough for the laboratory investigation of three-dimensional fish-like swimming.

Table of Contents

References

[1] F. Berlinger, J. Dusek, M. Gauci, and R. Nagpal, "Robust maneuverability of a miniature, low-cost underwater robot using multiple fin actuation," *IEEE Robotics and Automation Letters,* vol. 3, no. 1, pp. 140-147, 2017.

[2] A. Mathis *et al.*, "DeepLabCut: markerless pose estimation of user-defined body parts with deep learning," Nature Publishing Group, 1546-1726, 2018.

1 Harvard University John A. Paulson School of Engineering and Applied Sciences, Cambridge, MA 02138, USA
2 Department of Organismal and Evolutionary Biology, Harvard University, Cambridge, MA 02138, USA
3 College of Engineering and Computing, University of South Carolina, Columbia, SC 29208, USA
* Corresponding author: fberlinger@seas.harvard.edu

1 The Finbot Platform

Finbot combines high degrees of autonomy, maneuverability, and biomimicry with miniature size. It is exceptionally suitable for controlled three-dimensional (3D) experiments on fish-like swimming in confined laboratory test beds. The robot design builds on our own previous work [1] and has several distinctive features in comparison to other fish-like robotic platforms (Table S1).

Platform	Autonomy	Maneuverability	Biomimicry	Size
Finbot	Power, sensing, control, actuation	3D, 4DoF, 4 fins (lab)	Speed-frequency, CoT, *wake*, St, body	160 cm^3 ≙ 1.0x
Robotic swimmer [29]	Power, actuation (RC)	2D, 1DoF, 1 fin (lab)	Body	85 cm^3 ≙ 0.5x
Robotic fish [27]	Power, actuation (RC)	2D, 1DoF, 1 fin (lab)	Body	295 cm^3 ≙ 1.8x
Tunabot [25]	Actuation (power tethers)	2D, 1DoF, 1 fin (positioning harness, lab)	Speed-frequency, CoT, *wake*, St, kinematics, body	306 cm^3 ≙ 2.9x
Robot fish [31]	Power, actuation (RC)	3D, 2DoF, 1 fin + 1 rudder (lab + open water)	Speed-frequency, St, kinematics, body	500 cm^3 ≙ 3.1x
iSplash-II [33]	Power, actuation	3D, 2DoF, 1 fin + 1 rudder (lab)	Speed-frequency, CoT, St, kinematics, body	835 cm^3 ≙ 5.2x
Biki (robosea.org)	Power, sensing, actuation (RC)	3D, 3DoF, 1 fin, BCU (open water)	Body	1,100 cm^3 ≙ 6.9x
SoFi [20]	Power, sensing, actuation (RC)	3D, 3DoF, 1 fin, 2 dive planes, BCU (open water)	Body	1,600 cm^3 ≙ 10x
GhostSwimmer [21]	Power, sensing, control, actuation	3D, 4DoF, 1 fin, BCU (open water)	Body	40,800 cm^3 ≙ 255x
Flapping props [14-17]	n/a, attached to *external* device	n/a, 1-2 *external* DoF (lab)	n/a, abstracted physical models	n/a (2D foils)

Table S1. Finbot is autonomous, maneuverable, and biomimetic at a small size. No other robot at Finbot's size has four independently controllable fins; wake structures were visualized with particle image velocimetry (PIV) for one previous robot only (Tunabot). Abbreviations: buoyancy control unit (BCU), cost of transport (CoT), degree of freedom (DoF), laboratory (lab), not applicable (n/a), propulsors (props), remote-controlled (RC), Strouhal number (St).

1.1 Multi-fin Maneuverability

A high degree of maneuverability is achieved by a multi-fin design that allows, for instance, controlled submerged straight-line swimming during which performance metrics can be measured (Section 2). A caudal fin provides thrust in forward direction along the surge-axis, and two pectoral fins effect on-the-spot turning in the horizontal surge-sway-plane. When run together, the pectoral fins provide thrust in negative surge-direction and allow for stopping and backing up

since we angled them 30° forward against the sway-axis for this study. Vertical ascent and descent are decoupled from planar motions. Finbot is slightly positively buoyant and floating toward the surface unless the dorsal fin is actuated [1]. The dorsal fin generates thrust along the heave-axis and allows for controlled diving, using feedback from a pressure sensor (TE connectivity MS5803-02BA).

1.2 Electromagnetic Actuators

All four fins are powered by our custom magnet-in-coil actuators (MICs), which are made from an electromagnetic coil inside which a permanent magnet is hinged [1]. Oscillating the direction of an electric current flowing through the coil induces an oscillating magnetic field, with which the magnet tries to stay aligned. As a result, the fins oscillate around a single axis in a sinusoidal pitching motion. Changing the voltage across the coil with pulse width modulation (PWM) allows to adjust the electrical power available to the fins. The tail beat frequency follows the frequency of the oscillating current and is controlled by an H-bridge motor driver (Texas Instruments L293). The housings were updated and are now 3D-printed (Stratasys PolyJet Objet500) in the assembled state, i.e., including the pivoted hinge to which fins, laser-cut from flexible plastic shims (Artus corp), are attached. The caudal and the dorsal actuators were redesigned compared to the previous robot platform described in [1]. Here, they are equipped with two MICs each for enhanced propulsive force and connect magnetically to the robot body. The magnetic connection allows for fast switching between different fins, for instance to find caudal fins that result in effective locomotion. An exploded view of a caudal actuator and the caudal peduncle are shown in Fig. S1A-B.

1.3 Onboard Electronics

Finbot is equipped with multiple sensors and an onboard microcontroller (Arduino Pro Mini 238) to enable self-propelled and controlled swimming. All electronic components are connected to a newly designed printed circuit board (PCB, OSH Park). Two 7.4 V 280 mAh batteries (E-flite) provide power for run times of up to 2.3 h. The onboard voltage is reduced to 5 V by a step-down voltage regulator (Pololu D24V50F5). Finbot is switched on and off with a waterproof slide switch (TE Connectivity 1825032-1). One USB port is used for charging and programming (Molex 0483930003). Programs are written in C++ and typically loop at a frequency of about 30 Hz. Write operations for data logging on a microSD card (Sparkfun DEV-13743) are the speed limiting factor. An inertial measurement unit (InvenSense MPU-9250) is used for ego-pose estimation, in particular for straight-line swimming. Finally, a power monitor (Texas Instruments INA219) measures the input power, P, to the caudal fin. Power, together with measured speed, U, and known mass, m, is important to derive the cost of transport, $CoT = P/mgU$.

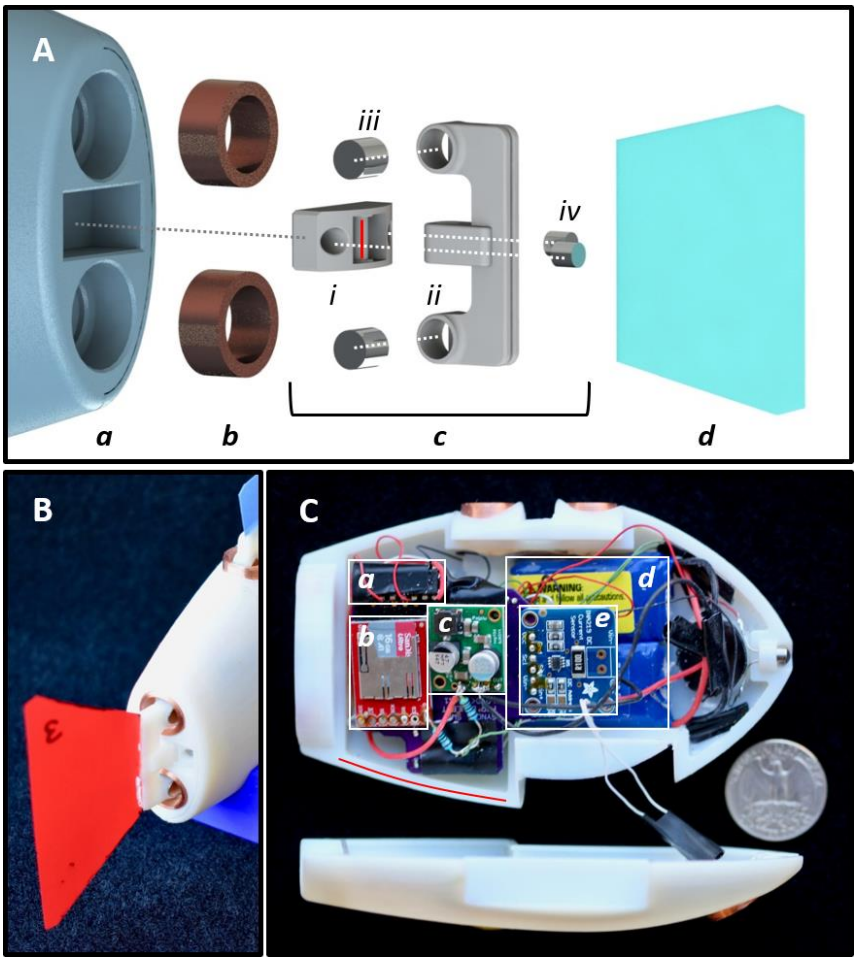

Fig. S1. Finbot's caudal actuator and interior. (A-B) The caudal peduncle features a magnetic connector to which different actuators and fins can be attached. (A) Exploded view of a caudal actuator: Two electromagnetic coils (b) are permanently installed at the caudal peduncle (a), and their stationary wires connect to the inside of the robot. The exchangeable caudal actuators consist of a pivoted hinge (c) to which a passive fin (d) is attached. The stator (i) and rotor (ii) are 3D-printed as a single part, whereby the rotor is free to rotate about the vertical shaft indicated in red. Two permanent magnets with agreeing axial polarities (iii) are mounted on the rotor, and two permanent magnets with opposite axial polarities (iv) on the stator. The latter (iv) are matched by two magnets on the inside of the caudal peduncle (a), and enable a resealable connection between the peduncle (a) and the actuator (c,d). The former (iii) come to sit inside the electromagnetic coils (b), and thus we term our actuator the magnet-in-coil (MIC) actuator. (C) The inside of a preassembled Finbot: All the electronics are mounted inside the left hull, including 3 H-bridge motor drivers (a), an SD card reader/writer (b), a 5 V voltage regulator (c), two 7.4 V 280 mAh batteries (d), and a power monitor (e). An Arduino microcontroller and an IMU are soldered to the hidden bottom side of a custom-made PCB. The assembly is completed by applying plastic-bonding epoxy on the peripheral sealing lip (bottom left section indicated in red) and closing the robot with the right hull.

1.4 Robot Assembly

The complete assembly of Finbot takes four hours. First, all actuators and the electronics inside the two 3D-printed plastic halves are installed. Then, electronic components are soldered to the PCB, and those penetrating the body are sealed from the inside. Finally, the two halves are fused into a single robot using plastic bonding epoxy (Loctite Plastic Bonder). Careful placing of components such that the center of mass is directly below the center of buoyancy achieves passive stability in roll and pitch as well as near-neutral buoyancy. A newly added small compartment on the ventral side of Finbot, which is sealed from the rest of the body and opened with a single bolt, allows for the fine tuning of buoyancy with additional mass blocks. A preassembled Finbot including an inside view of the electronics is shown in Fig. S1C.

2 Closed-loop Controlled Multi-fin Free Swimming

Finbot has four independently controllable fins for a high degree of maneuverability in 3D space.

2.1 Planar Swimming

Finbot can maintain a submerged straight-line course by using feedback from an IMU to correct any deviations with the pectoral fins. The gains of the corresponding proportional–integral–derivative (PID) controller (Fig. S2) were found empirically in a flow tank, and the derivative gain was of particular importance due to the robot's inertia in water (Movie S3). The proportional gain was set such that a heading error of 5° resulted in maximal counteraction, i.e., a pectoral fin frequency of 8 Hz. The derivative gain was fixed to about one third of the proportional gain in order to smooth the control and avoid overshooting. The integrative gain was about 0.25 % of the proportional gain since it added up quickly with typical control and reading frequencies of about 30 Hz. Moreover, the magnitudes of the gains were adjusted according to swimming speeds to apply more aggressive control at higher speeds. Independent of the controller, small deviations from straight-line courses may occur and stem from drift on the IMU of approximately 0.5 °/min in yaw. We mitigated such deviations by subtracting steady-state drift measured during initialization at rest from continuous readings during swimming.

2.2 Vertical Diving

Diving along the vertical heave-axis is decoupled from planar motions and achieved with the dorsal fin using feedback from a pressure sensor. The pressure sensor used for controlled diving is free from drift and has sub-millimeter resolution in water, allowing for diving at a consistent target depth with sub-centimeter deviations in heave after control. The surface pressure, to which a target depth gets added, was measured during initialization at rest at the beginning of each experiment. The target depth for all experiments was set to 15 cm, i.e., centered between floor and water surface, and matched with the position of the laser light sheet for experiments including particle image velocimetry (PIV). During experiments, the diving was controlled to be constantly around 15 cm such that the laser light sheet remained positioned closely around the mid-body and mid-caudal span location (Fig. 1D in the main paper).

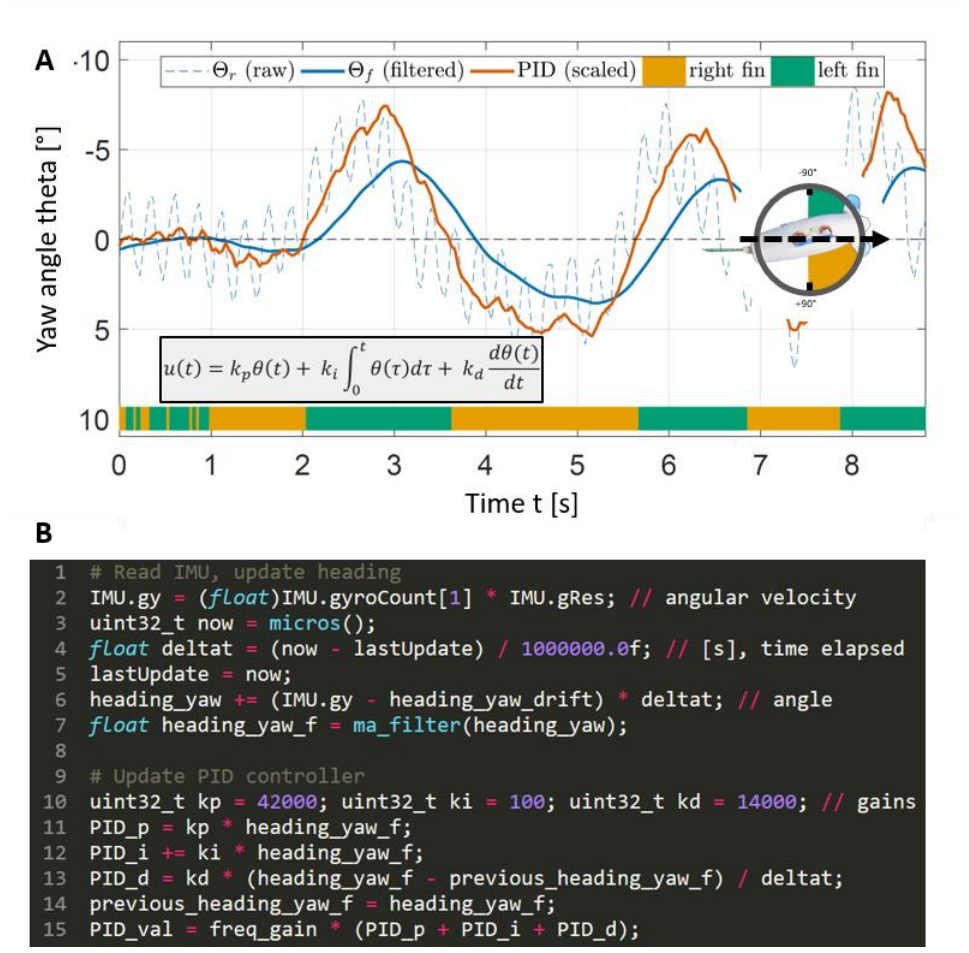

Fig. S2. Closed-loop controller design for the swimming of straight line trajectories. (A) Finbot operates at constant tail beat frequencies – 4Hz in this case – and uses its right and left pectoral fins to remain on a straight-line course. Raw heading data Θ_r is read from an IMU at a frequency of 30Hz (dashed blue line), enough to also sense recoil motions from oscillations of the tail. The raw data is then time-averaged to Θ_f (solid blue line), introducing some time delay. Based on Θ_f, the output $u(t)$ of a PID controller (see equation) is regulating the frequencies of the pectoral fins, whereby the right fin (orange) is active when the angular deviation from a straight line is positive, and the left fin (green) otherwise. The derivative component of the controller k_d is of particular importance to account for the robot's inertia and mitigate the time delay introduced by averaging the raw data. (B) The PID controller is implemented in C++. In every loop, the heading estimate is updated before the new controller output is derived. The gains (line 10) were tuned empirically. The frequency gain (line 15) is a number in the unit interval that adjusts the final control output according to the frequency of the caudal fin and the cruise speed of the robot, respectively. Higher speeds require more aggressive control.

3 Data Processing for Swimming Speed and Power Consumption

We conducted all the experiments in fresh water in a laboratory flow tank that consisted of a 66 cm x 28 cm x 28 cm (l, w, h) large test section (Fig. S3A).

3.1 Swimming Speed

Swimming speeds at steady-state cruise, i.e., after an initial acceleration period, were deducted from recorded videos. In order to achieve a high degree of repeatability and standardization in the way we analyzed video data, we trained a deep convolutional neural network (CNN) with DeepLabCut [2] to identify head, tail, and fin tip by manually labelling those three points of interest in 100 video frames. The trained CNN then found head, tail, and fin tip in new videos and outputted their respective pixel coordinates in each frame, from which we calculated cruise speed (Movie S4). Four instances during cruise at a tail beat frequency of 4 Hz are depicted in Fig. S3B. Drag force on Finbot's body scaled with speed squared, and the drag coefficient remained relatively constant at high speeds (Fig. S4A-B). An exemplary trajectory and fin tip amplitude transient are shown in Fig. S4C-D.

3.2 Power Consumption

The power consumption of the caudal fin for forward propulsion was measured with an onboard power monitor at a sampling rate of approximately 30 Hz. We averaged the sampled power values over the course of an experiment to report a single mean power since the actual power was pulse-width modulated at 980 Hz to achieve a desired actuation strength. The reported mean powers were found to match the expected theoretical means accurately despite sub-sampling the power signal. An exemplary power transient at a tail beat frequency of 4 Hz is shown in Fig. S4E.

The pectoral and dorsal fins as well as onboard electronics combined accounted for an additional power consumption on the same order of the caudal fin, thereby doubling the effective total power. However, the contributions of pectoral and dorsal fins along with electronics were neglected since they did not contribute to forward propulsion. Consequently, costs of transport must be understood as the cost of forward propulsion.

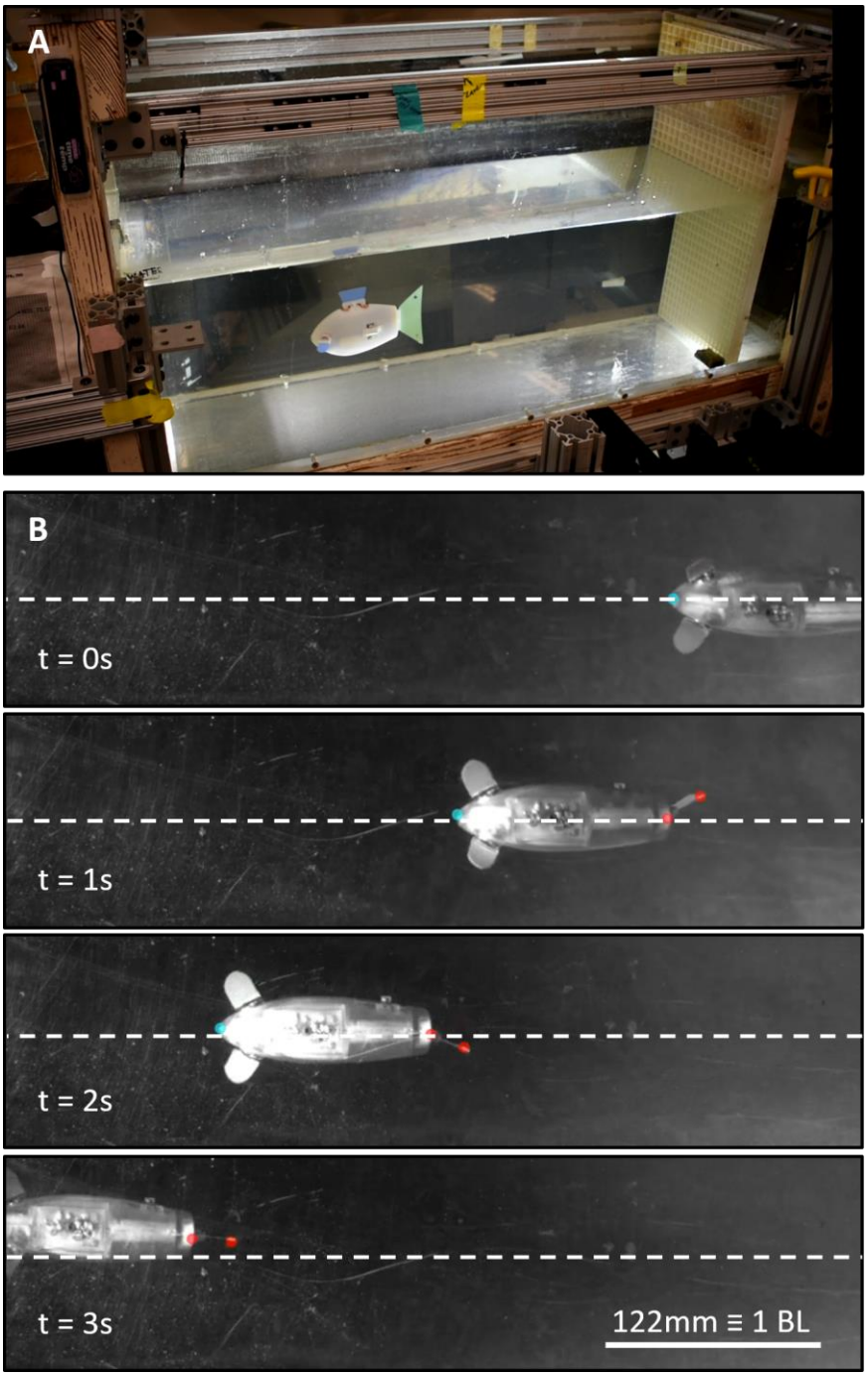

Fig. S3. Tracking and analysis of swimming speeds. (A) A perspective view on Finbot during an experiment in the tank, which was filmed with a camera mounted beneath. (B) Four instances of cruise for swimming at a tail beat frequency of 4Hz. The nominal straight-line trajectory is marked by a dashed white line.

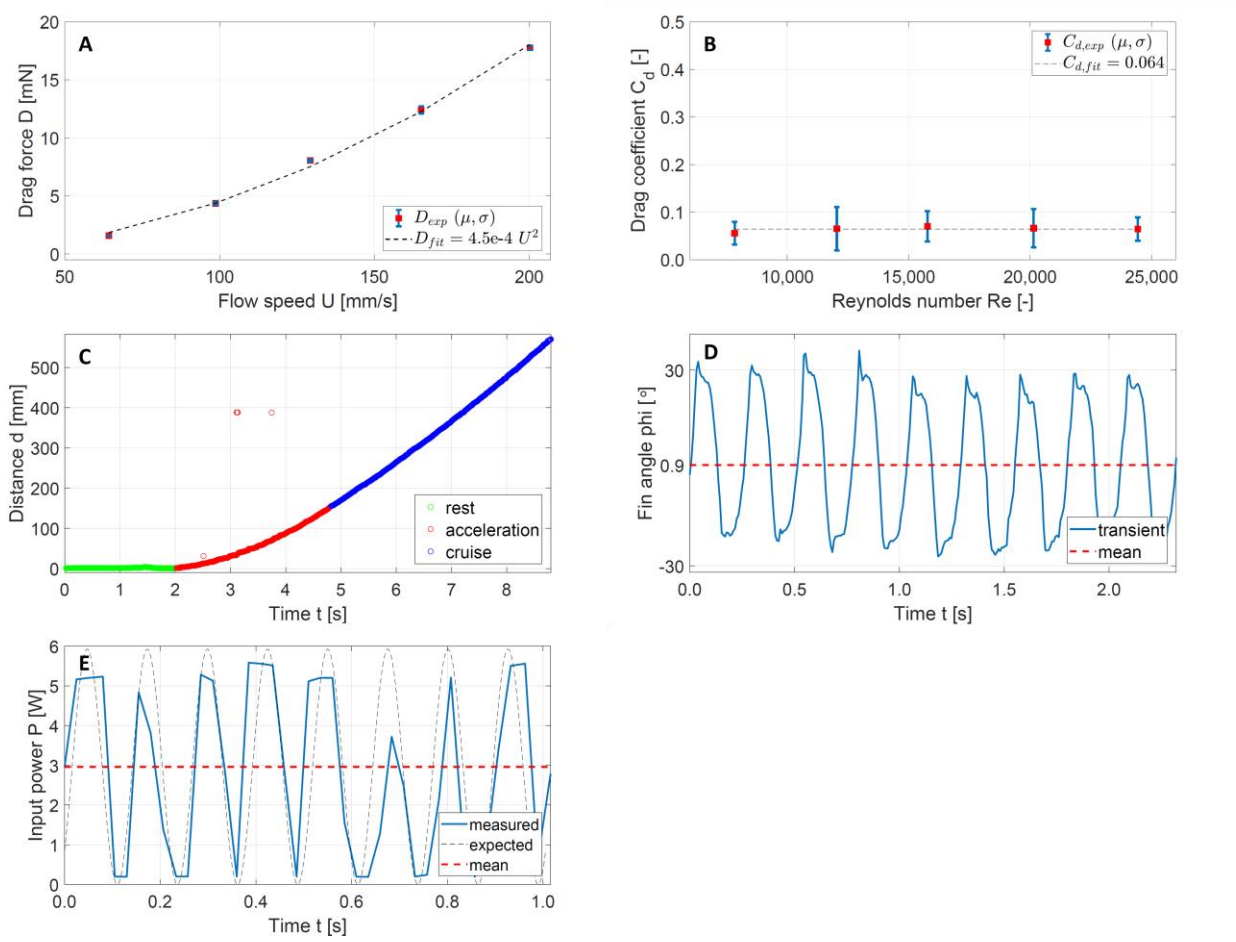

Fig. S4. Form drag, exemplary trajectory and fin tip transient, power measurement. (A) Drag force on Finbot's body scales with speed squared. (B) Drag coefficient remains relatively constant at high speeds. (A–B): Red squares are the mean μ of N = 5 trials. Blue error bars depict standard deviations σ from the mean, most of them obscured by the red square. The black dashed line represents a fitted curve. (C) An exemplary trajectory of Finbot swimming at a tail beat frequency of 4Hz. The robot is initialized at rest (green), goes through a period of acceleration (red, 2s–4.8s), and reaches cruise speed (blue), which we reported in all speed-related graphs. (D) The fin tip transient corresponding to (C). The caudal fin was set to symmetrically oscillate between ±30° (blue solid line). In order to swim straight, the offset of 0.9° (red dashed line) – likely due to assembly imperfections – can be compensated by closed-loop control using the pectoral fins together with feedback from an IMU. (E) Measured input power corresponding to (C). The prescribed signal (black dashed line) is sinusoidal, oscillating at 8Hz in order to complete 4 peak-to-peak amplitudes within 1 second. The reported mean power (red dashed line) matches the expected mean of the prescribed signal accurately despite measuring power (blue solid line) at a sub-sampled rate.

4 Additional Wake Structures from Particle Image Velocimetry

We used PIV to visualize and analyze Finbot's swimming performance. Fig. S5A shows Finbot swimming through illuminated particles with its diving depth carefully tuned and controlled such that the laser light sheet is positioned at the mid-body and mid-caudal span location. We also analyzed the streamlines surrounding Finbot and found detached flow at the posterior end in the region of the caudal peduncle (Fig. S5B). Such detached flow hinders swimming performance as it increases form drag, but was an unavoidable consequence of the current Finbot design. Moreover, it appears in areas where the caudal fin is flapping and therefore potentially reduces thrust production. Currently limited by the actuator desgin, a more markedly reduced cross-sectional area of the caudal penduncle might improve overall performance.

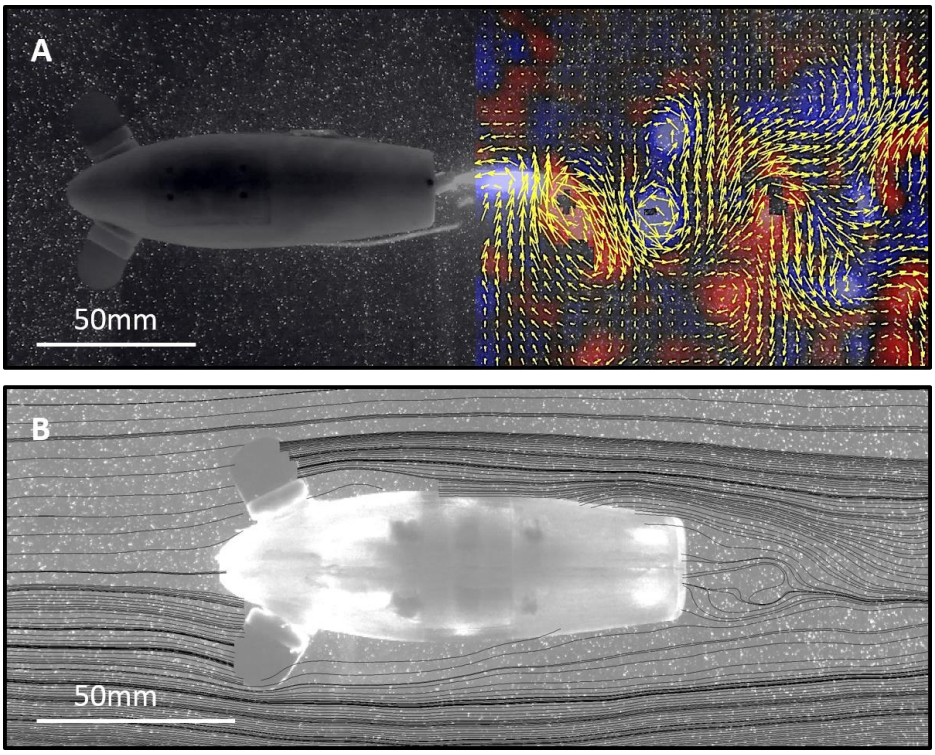

Fig. S5. Particle image velocimetry. (A) Visualization of wake structures. Red and blue colors indicate opposite sign vorticity. Yellow arrows show flow velocity vectors. (B) Visualization of streamlines (black lines) shown over a PIV image of Finbot during cruise.

4.1 Wake Strutures of Twelve Tested Fins

Here we show the wake structures for all twelve fins from Fig. 3a in the main paper. Strength and directionality of wakes varied considerably among the fins (Fig. S6). Bifurcated wakes with large opening angles (e.g. fins 2, 5) are less effective than reversely directed Kármán-like wakes (e.g. fins 7, 11) due to lateral losses. Looking at the wakes of different fins at a single actuation frequency, however, can only offer an isolated and limited view on fin optimality since optimal actuation frequencies are fin-specific. Fin 11 was selected due to its fish-like wake structure as one of five fins for a detailed performance investigation across several tail beat frequencies.

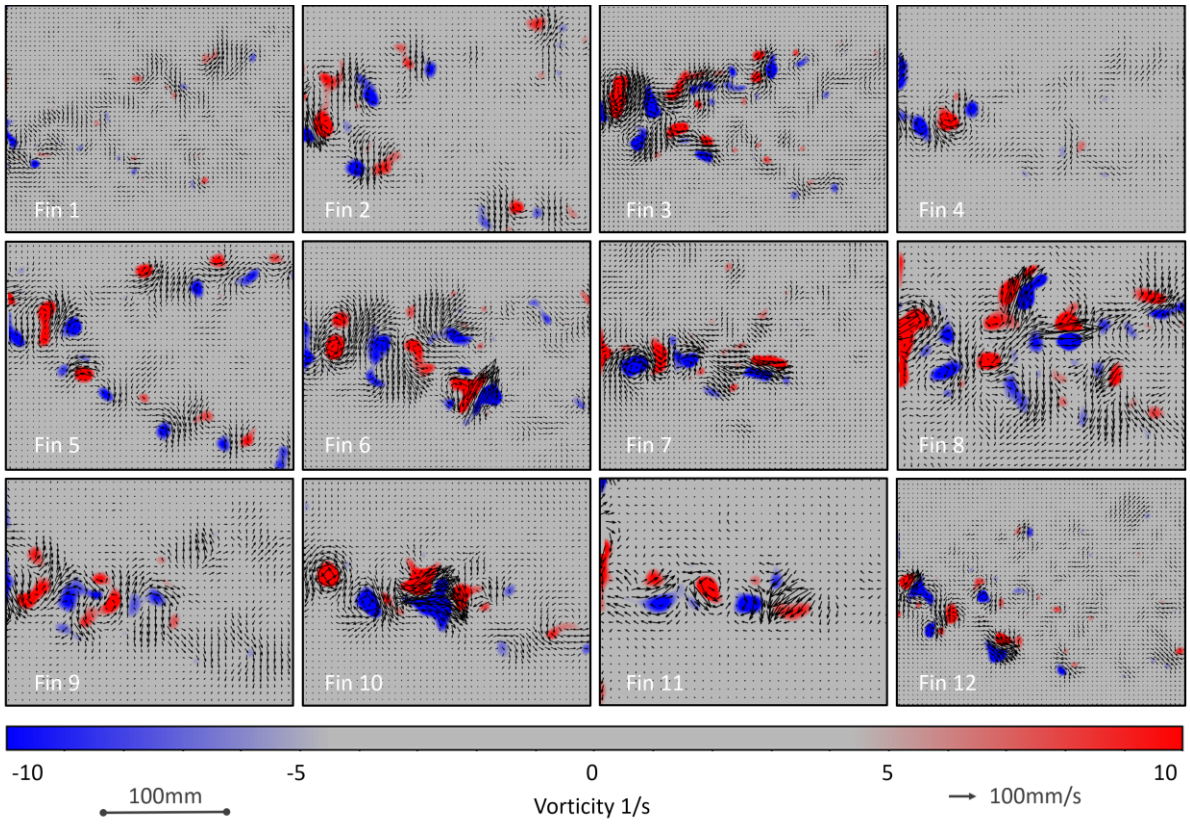

Fig. S6. Wake structures of twelve tested fins at a tail beat frequency of 2Hz.

4.2 Wake Structures of Fin 6

We further tested fin 6 for a wider range of tail beat frequencies and CoTs (Fig. S7). The curve for cost of transport across seven actuation frequencies spanning from 1Hz to 4Hz is U-shaped (top left). The corresponding wakes at each frequency and CoT, respectively, are shown in the subsequent seven images. More ideal reverse Kármán wakes correspond to lower CoTs and intermediate frequencies (e.g. f = 2.5Hz, CoT = 13.8). Less effective bifurcated wakes with reduced thrust appear at extreme frequencies (low and high) and suboptimal CoTs (particularly at f = 1Hz, CoT = 19.5).

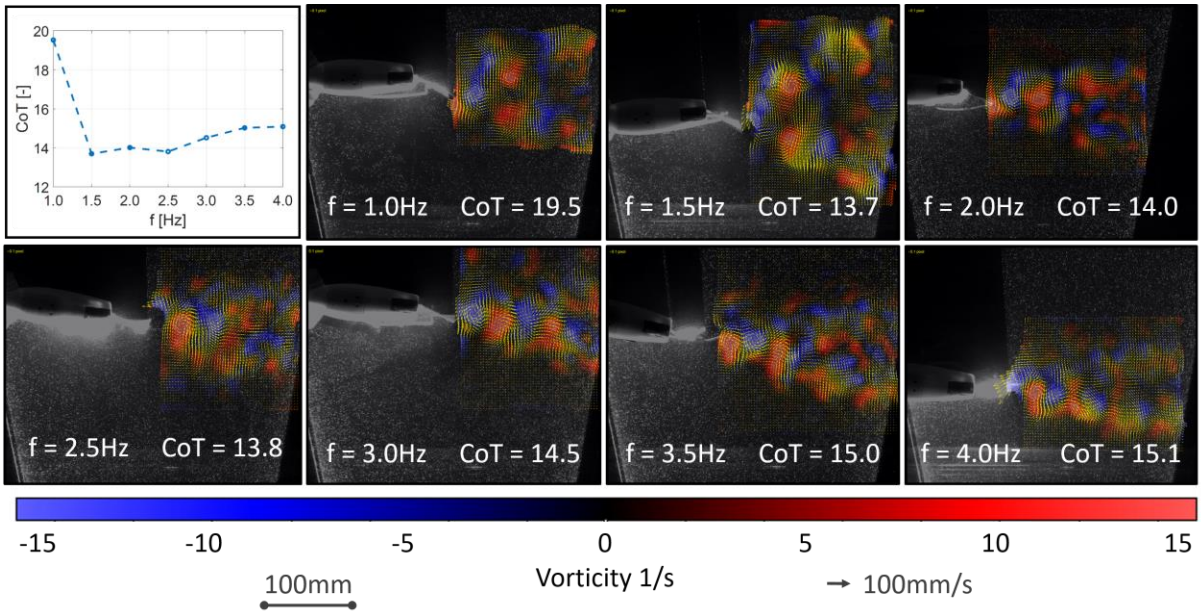

Fig. S7. Wake structures of fin 6 for a wider range of tail beat frequencies and CoTs.

5 From Battery Power to Forward Speed

Compared to real fish, Finbot's locomotion is inefficient and results in a higher CoT. For Finbot, the generation of forward speed from battery power depends on three components. First, the custom magnet-in-coil actuator (MIC) consumes electrical power and generates torque on the hinge to which the fin is attached. The torque-to-input-power ratio depends on the parameters of the MIC, such as permanent magnet strength, coil current, and magnet and coil dimensions (see supplement of [1]). Second, the torque is "converted" into thrust by the fin. The efficiency of this process is influenced by fin size, shape, and material properties, as well as by the amplitude and frequency of oscillation. Third, the cruise speed that Finbot can reach for a given thrust is a function of the hydrodynamic properties of its body. We mainly attribute the efficiency losses to the first component, i.e., the ineffective conversion from battery power to fin oscillations in our MIC actuators. Since the rotational speed of the magnet inside the coil is very small, operating the MIC actuator is analogous to operating a DC motor at stall torque, which is known to be highly inefficient.